Entanglement distribution over quantum code-division multiple-access networks

Chang-long Zhu,[1,2] Nan Yang,[1,2] Yu-xi Liu,[2,3] Franco Nori,[4,5] and Jing Zhang[1,2,*]

[1]*Department of Automation, Tsinghua University, Beijing 100084, People's Republic of China*

[2]*Center for Quantum Information Science and Technology, TNList, Beijing 100084, People's Republic of China*

[3]*Institute of Microelectronics, Tsinghua University, Beijing 100084, People's Republic of China*

[4]*CEMS, RIKEN, Saitama 351-0198, Japan*

[5]*Department of Physics, University of Michigan, Ann Arbor, Michigan 48109-1040, USA*

(Received 9 July 2015; published 26 October 2015)

We present a method for quantum entanglement distribution over a so-called code-division multiple-access network, in which two pairs of users share the same quantum channel to transmit information. The main idea of this method is to use different broadband chaotic phase shifts, generated by electro-optic modulators and chaotic Colpitts circuits, to encode the information-bearing quantum signals coming from different users and then recover the masked quantum signals at the receiver side by imposing opposite chaotic phase shifts. The chaotic phase shifts given to different pairs of users are almost uncorrelated due to the randomness of chaos and thus the quantum signals from different pair of users can be distinguished even when they are sent via the same quantum channel. It is shown that two maximally entangled states can be generated between two pairs of users by our method mediated by bright coherent lights, which can be more easily implemented in experiments compared with single-photon lights. Our method is robust under the channel noises if only the decay rates of the information-bearing fields induced by the channel noises are not quite high. Our study opens up new perspectives for addressing and transmitting quantum information in future quantum networks.

DOI: 10.1103/PhysRevA.92.042327 PACS number(s): 42.50.Ex, 03.67.Bg, 62.25.Jk, 89.70.−a

I. INTRODUCTION

With recent progress in various quantum systems such as ion-trap systems [1–3] and solid-state quantum circuits [4–6], it is now possible to discuss how to establish more efficient quantum networks or a so-called quantum internet [7]. Previous studies about quantum communication [8–10] and quantum cryptography [11,12] have shown that quantum network has great advantages to transfer classical or quantum information. However, how to best transfer information via quantum networks is still an open problem [13–23].

In transferring quantum information over a large-scale quantum network, a question that is asked is whether we can allow different pairs of users, who want to transmit information, to share the same channel [24–26]. This problem has been widely discussed in the field of classical communication [27,28]. In classical communication systems, such methods are called channel-access methods or multiple-access methods. There are mainly four different kinds of multiple-access methods [29]: the frequency-division multiple-access (FDMA) methods, the time-division multiple-access (TDMA) methods, the code-division multiple-access (CDMA) methods, and the orthogonal frequency-division multiple-access (OFDMA) methods. In FDMA methods, different frequency bands are assigned to different data streams, while in TDMA methods the users split their signals into pieces and transmit them at different time slots to share the same channel. The TDMA and FDMA methods work equally well and are the key techniques for the first-generation (analog) and the second-generation (digital) mobile networks. In CDMA methods, each pair of users shares the same channel and distinguishes each other by their own unique codes. It can be shown that the CDMA method can accommodate more bits per channel use, compared with the TDMA and FDMA [30] methods, and thus is used in third-generation mobile communication systems. However, the interference between different data streams will deteriorate the information rate of the CDMA method. Other competitive approaches are proposed including the OFDMA method, in which the available subcarriers are divided into several mutually orthogonal subchannels that are assigned to distinct users for simultaneous transmission. The OFDMA method is capable of avoiding the interference problem and thus provides better performance in classical *digital* communication.

Although the multiple-access problem has been widely studied in classical communication, it has been considered in quantum communication only recently due to the development of techniques for a scalable quantum network. The FDMA method, or, equivalently, the so-called wavelength-division multiple access method, has been used for quantum key distribution [31–36], in which classical information is transmitted over a quantum network, and the TDMA method has been used to generate large entangled cluster states [37]. However, whether more popular classical communication techniques such as the OFDMA [38,39] and CDMA [40–43] methods can be applied to quantum communication systems is still an interesting problem yet to be solved.

Recently, various protocols were proposed to extend the CDMA model to the quantum case [40–43] and there is evidence showing that the CDMA model can provide higher information rates for quantum communication compared with the FDMA model [40]. In Ref. [40], particular chaotic phase shifts, which work as a unique code in the CDMA model, are introduced to spread the information-bearing quantum signals in the frequency regime. Since the chaotic phase shifts introduced for different users are uncorrelated, the cryptographic quantum signals from different users are orthogonal and thus can be distinguished even when we transmit them via the same

*jing-zhang@mail.tsinghua.edu.cn

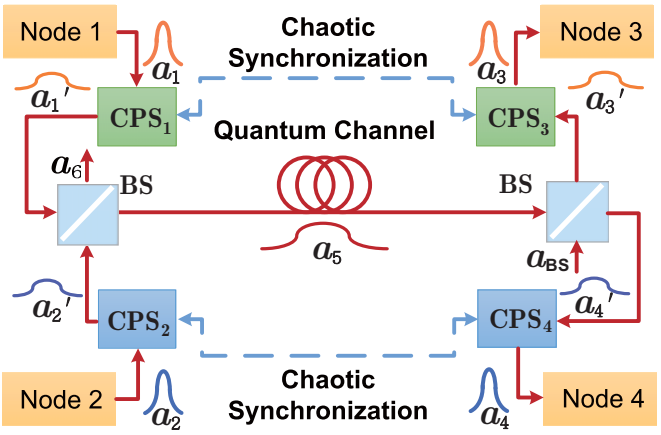

FIG. 1. (Color online) Schematic diagram of the quantum CDMA network by chaotic synchronization. The wave packets are broadened by two chaotic phase shifters, i.e., CPS_1 and CPS_2, at the senders, and then recovered by another two chaotic phase shifters, i.e., CPS_3 and CPS_4, at the receiver side.

channel. The cryptographic quantum signals can be decoded by introducing reversed chaotic phase shifts at the receiver side, by which the transmitted quantum information can be recovered coherently. The physical media used in Ref. [40] to transmit quantum information are single-photon lights [42].

Different from the protocol in Ref. [40], instead of single-photon lights we use bright coherent lights [43] to transmit quantum information over a quantum CDMA network, which is easier to realize in experiments. We find that quantum entanglement can be controllably distributed between two pairs of users sharing a single quantum channel. We also present the particular design of the chaotic phase shifters used in our proposal by introducing electro-optic modulators (EOMs) and chaotic Colpitts oscillator circuits [44], which are not clearly discussed in Ref. [40]. The Pecora-Carrol synchronization technique [45,46] is introduced to generate the reverse chaotic phase shifts at the receiver side. This paper is organized as follows. In Sec. II we present the general description of the quantum CDMA network we use to transmit quantum information. In Sec. III we state how to distribute maximally entangled quantum states over the proposed quantum CDMA network mediated by bright coherent lights. In Sec. IV we consider the nonideal case to see how channel noise will affect our main results. In Sec. V we summarize and present a forecast of future work.

II. QUANTUM CDMA NETWORK BY CHAOTIC SYNCHRONIZATION

The main purpose of our work is to generate two maximally entangled states between two pairs of nodes (one pair consists of nodes 1 and 3 and the second pair consists of nodes 2 and 4) via a single quantum channel (see Fig. 1). The quantum signals sent by nodes 1 and 2 are first encoded by two chaotic phase shifters CPS_1 and CPS_2 and the two output beams are combined by a 50:50 beam splitter and then transmitted via a quantum channel. At the receiver side, this combined quantum signal is divided into two branches by another 50:50 beam splitter and sent to another two chaotic phase shifters CPS_3 and CPS_4 introduced to decode the information. The recovered quantum signals are then sent to the two receiver nodes.

To understand the encoding and decoding processes of our method, let us assume that the optical field entering the ith chaotic phase shifter is a_i ($i = 1,2,3,4$). The chaotic phase shifter CPS_1 (CPS_2) induces an effective Hamiltonian $\delta_1(t)a_1^\dagger a_1$ [$\delta_2(t)a_2^\dagger a_2$], where $\delta_1(t)$ [$\delta_2(t)$] is a classical chaotic signal. It can be shown that CPS_1 (CPS_2) leads to phase-shift factor $\exp[-i\theta_1(t)]$ ($\exp[-i\theta_2(t)]$) for the optical field. At the receiver side, the chaotic phase shifter CPS_3 (CPS_4) induces the opposite Hamiltonian $-\delta_1(t)a_3^\dagger a_3$ [$-\delta_2(t)a_4^\dagger a_4$] by which a reversed phase-shift factor $\exp[i\theta_1(t)]$ ($\exp[i\theta_2(t)]$) is introduced to decode the information-bearing signal masked by the chaotic phase shift. Here $\theta_i = \int_0^t \delta_i(t)dt$, $i = 1,2$. To ensure that the chaotic phase shift at the sender side and that at the receiver side can be exactly canceled, an auxiliary classical channel between node 1 (node 2) and node 3 (node 4) is introduced to synchronize the two chaotic phase shifters [47,48] (see Fig. 1).

The whole information transmission process can be represented by the input-output relationship of the whole quantum network from a_1,a_2 to a_3,a_4 (see Fig. 1). To derive it, we can see that the input-output response of the chaotic phase shifters CPS_i, $i = 1,2,3,4$, can be written as

$$\begin{aligned} a_1' &= a_1 e^{-i\theta_1}, \quad a_2' = a_2 e^{-i\theta_2}, \\ a_3 &= a_3' e^{i\theta_1}, \quad a_4 = a_4' e^{i\theta_2} \end{aligned} \tag{1}$$

and the input-output response of the two beam splitters BS_1 and BS_2 can be written, respectively, as follows:

$$a_5 = \frac{1}{\sqrt{2}}a_1' + \frac{1}{\sqrt{2}}a_2', \quad a_6 = \frac{1}{\sqrt{2}}a_1' - \frac{1}{\sqrt{2}}a_2', \tag{2}$$

$$a_3' = \frac{1}{\sqrt{2}}a_5 + \frac{1}{\sqrt{2}}a_{BS}, \quad a_4' = \frac{1}{\sqrt{2}}a_5 - \frac{1}{\sqrt{2}}a_{BS}. \tag{3}$$

Hence, from Eqs. (1)–(3) we can obtain the input-output relationship of the whole quantum network

$$\begin{aligned} a_3 &= \frac{1}{2}a_1 + \frac{1}{2}a_2 e^{i(\theta_1-\theta_2)} + \frac{1}{\sqrt{2}}e^{i\theta_1}a_{BS}, \\ a_4 &= \frac{1}{2}a_2 + \frac{1}{2}a_1 e^{i(\theta_2-\theta_1)} - \frac{1}{\sqrt{2}}e^{i\theta_2}a_{BS}. \end{aligned} \tag{4}$$

For the chaotic phase shifts $\theta_i(t)$, $i = 1,2$, we should take the average over these broadband random phases [49], by which we have $\overline{\exp[\pm i\theta_i(t)]} \approx \sqrt{M_i}$ [50–52], where

$$M_i = \exp\left[-\pi \int_{\omega_{li}}^{\omega_{ui}} d\omega S_{\delta_i}(\omega)/\omega^2\right], \tag{5}$$

where $S_{\delta_i}(\omega)$ is the power spectrum density of the signal $\delta_i(t)$ and ω_{li} and ω_{ui} are the lower and upper bounds of the frequency band of $\delta_i(t)$, respectively. Equation (4) can then be reduced to

$$\begin{aligned} a_3 &= \frac{1}{2}a_1 + \frac{\sqrt{M_1 M_2}}{2}a_2 + \sqrt{\frac{M_1}{2}}a_{BS}, \\ a_4 &= \frac{1}{2}a_2 + \frac{\sqrt{M_1 M_2}}{2}a_1 - \sqrt{\frac{M_2}{2}}a_{BS}. \end{aligned} \tag{6}$$

The correction factor M_i may become extremely small when $\delta_i(t)$ is induced by a chaotic signal that has a broadband frequency spectrum. Thus we have $a_3 \approx a_1/2$ and $a_4 \approx a_2/2$, which means that the quantum signal transmitted from node 1 to node 3 and the quantum signal transmitted from node 2 to node 4 can be totally decoupled from each other even though they are transmitted simultaneously on the same quantum channel. The mechanism of such a quantum multiple-access network is that the information-bearing fields transmitted on the quantum channel are broadened by the chaotic phase shifters in the frequency regime, which cannot be detected unless we can reduce the chaotic phase shifts and sharpen the quantum signal by chaotic synchronization. This idea is quite similar to the classical CDMA communication. That is why we call it the quantum CDMA network in Ref. [40].

Now let us consider the case where the quantum fields a_1 and a_2 are in the coherent states $|\alpha_1\rangle$ and $|\alpha_2\rangle$ and the field $a_{\rm BS}$ is in a vacuum state. It can be easily checked from the input-output relationship given by Eq. (6) that the output fields a_3 and a_4 of the quantum network are in the coherent states

$$\begin{aligned} |\alpha_3\rangle &= |\tfrac{1}{2}\alpha_1 + \tfrac{1}{2}\sqrt{M_1 M_2}\alpha_2\rangle \approx |\tfrac{1}{2}\alpha_1\rangle, \\ |\alpha_4\rangle &= |\tfrac{1}{2}\alpha_2 + \tfrac{1}{2}\sqrt{M_1 M_2}\alpha_1\rangle \approx |\tfrac{1}{2}\alpha_2\rangle. \end{aligned} \tag{7}$$

III. QUANTUM ENTANGLEMENT DISTRIBUTION OVER THE QUANTUM CDMA NETWORK

Let us then consider how to distribute two-qubit quantum entanglement over the quantum CDMA network. In our proposal, the qubit states are stored in the dark states of four Λ-type three-level atoms in four optical cavities (see Fig. 2). What we want to do is generate a maximally entangled state between atom 1 (atom 2) and atom 3 (atom 4). Here we extend the strategy in Refs. [53,54] to generate such distributed entangled states by bright coherent lights. The Hamiltonian of the ith coupled atom-cavity system can be expressed as

$$\tilde{H}_i^{\rm QC} = \omega_c a_i^\dagger a_i + \frac{\omega_q}{2}\sigma_z^{(i)} + g(a_i^\dagger \sigma_-^{(i)} + a_i \sigma_+^{(i)}), \tag{8}$$

where ω_c and a_i ($a_i^\dagger$) are the frequency and the annihilation (creation) operator of the cavity mode; ω_q, $\sigma_z^{(i)}$, and $\sigma_\pm^{(i)}$ are the frequency, the z-axis Pauli operator, and the ladder operators of the qubit; and g is the coupling strength between the qubit and the cavity mode. Here, to simplify the discussion, we have assumed that the system parameters are the same for four-qubit-cavity systems. Under the dispersive-detuning condition $|\Delta| = |\omega_c - \omega_q| \gg |g|$, the Hamiltonian can be diagonalized and reexpressed in the interaction picture as [55]

$$H_i^{\rm QC} = \frac{g^2}{\Delta} a_i^\dagger a_i \sigma_z^{(i)}. \tag{9}$$

In this paper we introduce four EOMs [56] acting as the chaotic phase shifters CPS_i. It is known that the refractive index of the electro-optic crystal in the EOM can be varied by changing the voltage $V(t)$ acting on it [see Fig. 3(a)]. Based on this effect, we let the information-bearing optical field pass through the EOM to obtain a phase shift β, which will be changed by varying the voltage $V(t)$ acting on it. This phase shift can be expressed as $\beta = (\omega n^3 r L/cd)V(t)$, where ω is the frequency of the injected light n is the refractive index and the electro-optic coefficient of the electro-optic crystal in the EOM, L and d are the length and thickness of the EOM [see Fig. 3(a)], respectively, and c is the velocity of light. Therefore, when the optical field transmits through the EOM, an interaction Hamiltonian $H_i = \delta_i(t) a_i^\dagger a_i = -(\hbar/\tau)\beta a_i^\dagger a_i$ [57] can be obtained, where a_i ($a_i^\dagger$) is the annihilation (creation) operator of the injected field and τ is the optical round-trip time through the EOM. In the present system, each pair of EOMs is driven by two synchronized standard chaotic Colpitts oscillator circuits, as shown in Fig. 3(b), and the specific synchronized circuit is presented in Appendix A. We use the voltage V_{C2} to drive one EOM at the sender side and the voltage $\tilde{V}_{C2}$ to drive another EOM at the receiver side, as shown in Fig. 3(b).

To show how the quantum entanglement is distributed over our quantum CDMA network, we assume that the ith atom is in a superposition state $|\psi_i\rangle = (|g_i\rangle + |e_i\rangle)/\sqrt{2}$ ($i = 1,2,3,4$). The probe field entering cavity 1 (cavity 2) is a bright coherent light $|\alpha\rangle$ with average photon number $\bar{n} = |\alpha|^2 \gg 1$. When the probe field comes out of cavity 1 (cavity 2) at time τ', the system composed of atom 1 and the probe field fed out of cavity 1 is in an entangled state

$$e^{-iH_1^{\rm QC}\tau'}|\psi_1\rangle|\alpha\rangle = \frac{1}{\sqrt{2}}(|g_1\rangle|\alpha e^{-i\phi/2}\rangle + |e_1\rangle|\alpha e^{i\phi/2}\rangle). \tag{10}$$

Similarly, the system composed of atom 2 and the probe light fed out of cavity 2 is also in an entangled state

$$e^{-iH_2^{\rm QC}\tau'}|\psi_2\rangle|\alpha\rangle = \frac{1}{\sqrt{2}}(|g_2\rangle|\alpha e^{-i\phi/2}\rangle + |e_2\rangle|\alpha e^{i\phi/2}\rangle). \tag{11}$$

Here $H_1^{\rm QC}$ and $H_2^{\rm QC}$ are the Hamiltonians given by Eq. (9) and $\phi = 2g^2\tau'/\Delta$ is the phase shift of the probe field induced by the qubit-cavity coupling. Thus, the system composed of atoms 1 and 2 and the two probe lights before entering our quantum CDMA network is in a separable state

$$\begin{aligned} &\frac{1}{2}[|g_1 g_2\rangle|\alpha e^{-i\phi/2}\rangle|\alpha e^{-i\phi/2}\rangle + |e_1 g_2\rangle|\alpha e^{i\phi/2}\rangle|\alpha e^{-i\phi/2}\rangle \\ &\quad + |g_1 e_2\rangle|\alpha e^{-i\phi/2}\rangle|\alpha e^{i\phi/2}\rangle + |e_1 e_2\rangle|\alpha e^{i\phi/2}\rangle|\alpha e^{i\phi/2}\rangle]. \end{aligned}$$

From Eq. (7), the system composed of atoms 1 and 2 and those two probe fields that enter cavities 3 and 4 is in the state

$$\begin{aligned} |\Phi\rangle = &\left(\frac{1}{\sqrt{2}}|g_1\rangle\left|\frac{1}{2}\alpha e^{-i\phi/2}\right\rangle + \frac{1}{\sqrt{2}}|e_1\rangle\left|\frac{1}{2}\alpha e^{i\phi/2}\right\rangle\right) \\ &\times\left(\frac{1}{\sqrt{2}}|g_2\rangle\left|\frac{1}{2}\alpha e^{-i\phi/2}\right\rangle + \frac{1}{\sqrt{2}}|e_2\rangle\left|\frac{1}{2}\alpha e^{i\phi/2}\right\rangle\right). \end{aligned}$$

Here we have omitted those $\sqrt{M_1 M_2}$ terms since the factors M_1 and M_2 are negligibly small in the chaotic regime. After transmitting over the quantum CDMA network, the probe fields a_3 and a_4 interact with atoms 3 and 4 and the interaction times are both τ'. Thus, the state of the total system composed of four atoms and the optical fields fed out of the quantum

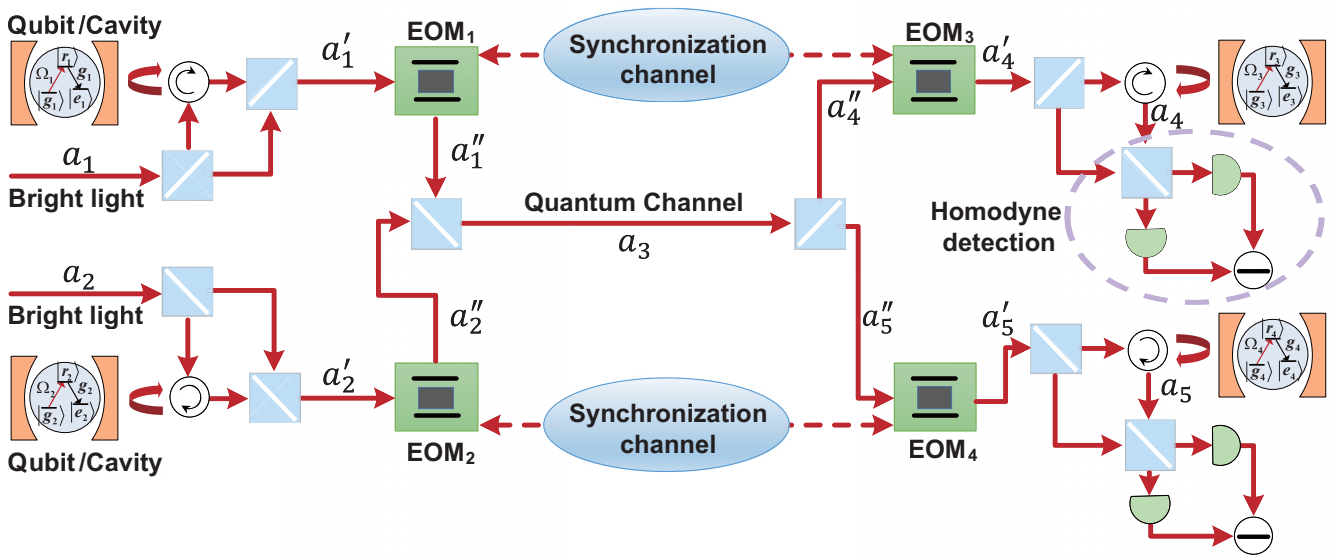

FIG. 2. (Color online) Schematic diagram of the entanglement distribution over a quantum multiple-access network. The bright coherent lights are sent to two cavities 1 and 2 in which the optical fields interact with atoms 1 and 2, respectively. After that, the two output beams transmit through two EOMs, i.e., EOM$_1$ and EOM$_2$, and are broadened in the frequency domain. The two output beams are then combined by an beam splitter and transmitted through a single quantum channel. At the receiver side, the combined optical field is split into two branches by another beam splitter and fed into another two EOMs, i.e., EOM$_3$ and EOM$_4$. Since the chaotic circuits driving EOM$_1$ (EOM$_2$) and EOM$_3$ (EOM$_4$) are synchronized, the chaotic phases introduced at the sender side can be compensated at the receiver side and thus the quantum signals transmitted can be recovered. The recovered quantum signals are then stored in the dark states of atoms 3 and 4 and homodyne detections are preformed for the output fields to postselect the maximally entangled states.

network is

$$
\begin{aligned}
&e^{-i(H_3^{\mathrm{QC}}+H_4^{\mathrm{QC}})\tau'}|\Phi\rangle\frac{1}{2}(|g_3\rangle+|e_3\rangle)(|g_4\rangle+|e_4\rangle)\\
&=\left(\frac{1}{\sqrt{2}}|\Psi_{13}^{+}\rangle\left|\frac{1}{2}\alpha\right\rangle+\frac{1}{2}|g_1g_3\rangle\left|\frac{1}{2}\alpha e^{-i\phi}\right\rangle\right.\\
&\quad\left.+\frac{1}{2}|e_1e_3\rangle\left|\frac{1}{2}\alpha e^{i\phi}\right\rangle\right)\\
&\quad\times\left(\frac{1}{\sqrt{2}}|\Psi_{24}^{+}\rangle\left|\frac{1}{2}\alpha\right\rangle+\frac{1}{2}|g_2g_4\rangle\left|\frac{1}{2}\alpha e^{-i\phi}\right\rangle\right.\\
&\quad\left.+\frac{1}{2}|e_2e_4\rangle\left|\frac{1}{2}\alpha e^{i\phi}\right\rangle\right),
\end{aligned}
\tag{12}
$$

where $|\Psi_{13}^{+}\rangle=(|g_1e_3\rangle+|e_1g_3\rangle)/\sqrt{2}$ is the maximally entangled state between atom 1 and atom 3 and $|\Psi_{24}^{+}\rangle=(|g_2e_4\rangle+|e_2g_4\rangle)/\sqrt{2}$ is the maximally entangled state between atom 2 and atom 4.

Finally, we impose homodyne detections on the probe fields leaking out of cavities 3 and 4. As shown in Eq. (12), the state of the probe fields leaking out of cavities 3 and 4 can be three possible states $|\alpha/2\rangle$, $|\alpha e^{-i\phi}/2\rangle$, and $|\alpha e^{i\phi}/2\rangle$. Since the probe fields are bright coherent lights with average photon number $\bar{n}=|\alpha|^2\gg 1$, we have

$$
\begin{aligned}
\left|\left\langle\tfrac{1}{2}\alpha\middle|\tfrac{1}{2}\alpha e^{-i\phi}\right\rangle\right|^2&=\exp[-\bar{n}\sin^2(\phi/2)]\approx 0,\\
\left|\left\langle\tfrac{1}{2}\alpha\middle|\tfrac{1}{2}\alpha e^{i\phi}\right\rangle\right|^2&=\exp[-\bar{n}\sin^2(\phi/2)]\approx 0,\\
\left|\left\langle\tfrac{1}{2}\alpha e^{-i\phi}\middle|\tfrac{1}{2}\alpha e^{i\phi}\right\rangle\right|^2&=\exp(-\bar{n}\sin^2\phi)\approx 0,
\end{aligned}
$$

which means that the three coherent states $|\alpha/2\rangle$, $|\alpha e^{-i\phi}/2\rangle$, and $|\alpha e^{i\phi}/2\rangle$ are pairwise orthogonal and thus completely distinguishable. Thus, the homodyne detections on the probe fields are just projective measurements. Corresponding to the three measurement outputs $\alpha/2$, $\alpha e^{-i\phi}/2$, and $\alpha e^{i\phi}/2$, the states of the system composed of atoms 1 and 3 (atoms 2 and 4) collapse to the maximally entangled state $|\Psi_{13}^{+}\rangle$ ($|\Psi_{24}^{+}\rangle$) and two separable states $|g_1g_3\rangle$ ($|g_2g_4\rangle$) and $|e_1e_3\rangle$ ($|e_2e_4\rangle$). The most important case is that the measurement outputs of the probe fields leaking out of cavities 3 and 4 are both $\alpha/2$. In this case, atoms 1 and 3 are in the maximally entangled state $|\Psi_{13}^{+}\rangle$ and atoms 2 and 4 are in the maximally entangled state $|\Psi_{24}^{+}\rangle$, which means that we generate two maximally entangled states between two pairs of nodes by sharing the same quantum channel.

We now consider the interference effects between the quantum signals from the two pairs of users. These interference effects have been omitted in our previous discussion under the condition that the correction factor M ($M=M_1M_2$) is negligibly small if the chaotic phases introduced have very broad bandwidths. However, these interference effects will affect the information transmission process if the bandwidths of the phase signals are not broad enough. To show this, let us consider how the correction factors M_1 and M_2 will change if we tune the correspondent bandwidths of the chaotic signals δ_1 and δ_2. From Fig. 4(a) we can see that both M_1 and M_2 decrease with an increase of the bandwidth of δ_1 and δ_2 and when we take the bandwidth values of the chaotic signals as 450 MHz, M_1 and M_2 are 0.0012 and 0.0033, respectively. With experimentally realizable parameters of the Colpitts chaotic circuits [45,46], it is not too difficult to generate a

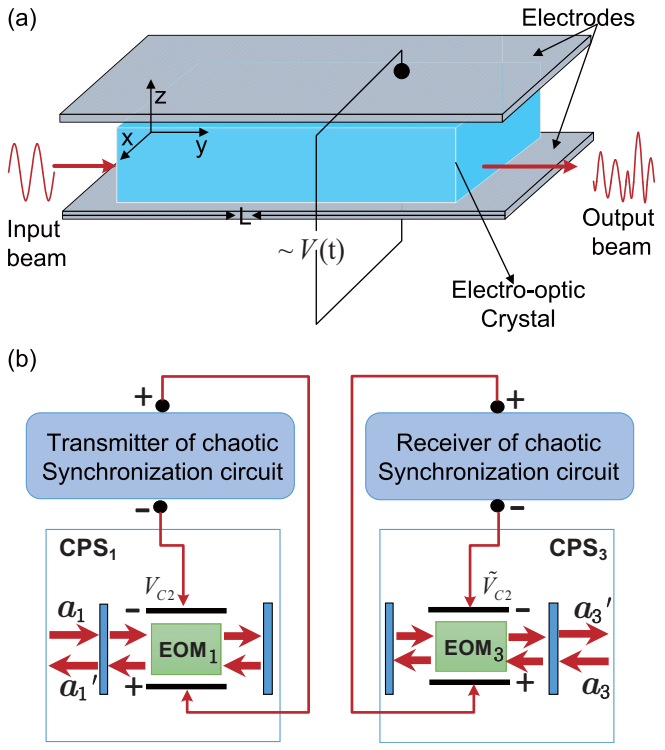

FIG. 3. (Color online) (a) Schematic diagram of a transverse electro-optic modulator. The voltage is applied perpendicular to the propagational direction of the input beam and the refractive index of the electro-optic crystal can be changed by varying the voltage V, which induces a voltage-dependent phase shift on the input beam. (b) Diagram of the chaotic synchronization circuit between CPS_1 and CPS_3, where the transmitter drives EOM_1 and the receiver drives EOM_3.

chaotic phase with bandwidth of 500 MHz and thus M_1 and M_2 can be very small. Meanwhile, we choose the average photon number $\bar{n} = 10$ and thus we have $M_1 M_2 \ll 4/\bar{n}$. This makes it reasonable to omit the $\sqrt{M_1 M_2}$ terms in Eqs. (6), (7), and (14). In order to check whether the phase shifts induced by the phase shifters are in the chaotic regime, we show in Fig. 4(b) the Lyapunov exponents of Colpitts circuits with different bandwidths. When the bandwidths of the Colpitts circuits are smaller than 100 MHz, the Lyapunov exponents of the Colpitts circuits are equal to zero, which means that these circuits work in the periodic regime. If we increase the bandwidths of the circuits, the Colpitts circuits will then enter the chaotic regime if the bandwidths are larger than 100 MHz, which corresponds to positive Lyapunov exponents [see Fig. 4(b)]. This is also confirmed by the phase diagrams and the power spectra of the circuits with a bandwidth of 100 MHz shown in Figs. 4(c) and 4(d) and those of the circuits with a bandwidth of 500 MHz in Figs. 4(e) and 4(f).

In order to show the efficiency of the entanglement distribution by the quantum CDMA network, we show in Fig. 5 the fidelities $F_1 = \langle \Psi_{13}^+ | \rho_{13} | \Psi_{13}^+ \rangle$ (see Appendix B) and $F_2 = \langle \Psi_{24}^+ | \rho_{24} | \Psi_{24}^+ \rangle$ versus the bandwidths of the chaotic signals and the average photon number of the probe fields $\bar{n}$, where $|\Psi_{13}^+\rangle$ ($|\Psi_{24}^+\rangle$) is the desired maximally entangled state between atoms 1 and 3 (atoms 2 and 4) and ρ_{13} (ρ_{24})

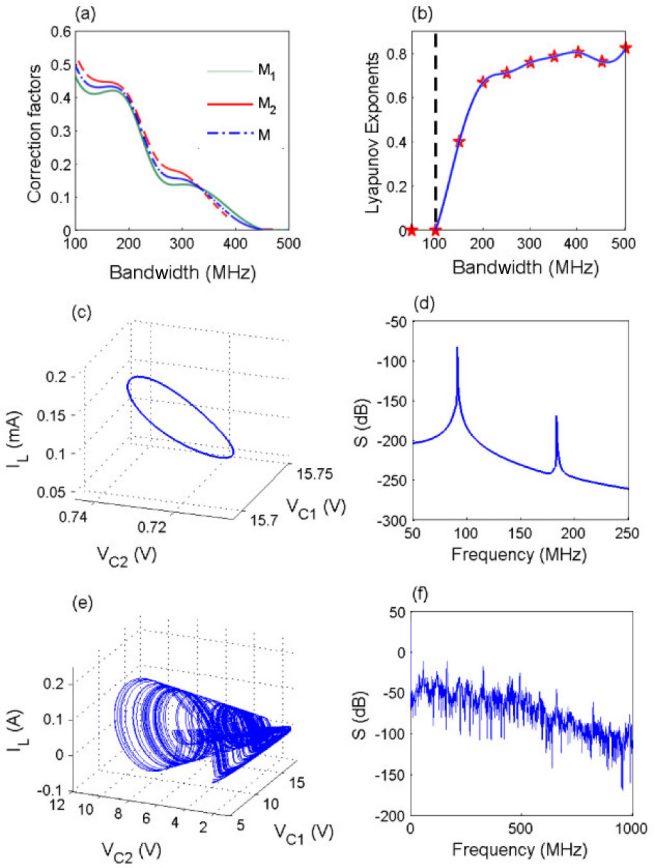

FIG. 4. (Color online) (a) Factors M_1, M_2, and M versus the bandwidths of the Colpitts circuits without channel noise. The green solid curve represents the factor M_1. The red dashed line denotes the curve for the factor M_2. The blue dash-dotted curve shows the factor $M = \sqrt{M_1 M_2}$. (b) Lyapunov exponents of the Colpitts circuits versus different bandwidths of the circuits. (c) Phase diagram and (d) power spectrum of the Colpitts circuit with a bandwidth 100 MHz. (e) Phase diagram and (f) power spectrum of the Colpitts circuit with a bandwidth of 500 MHz.

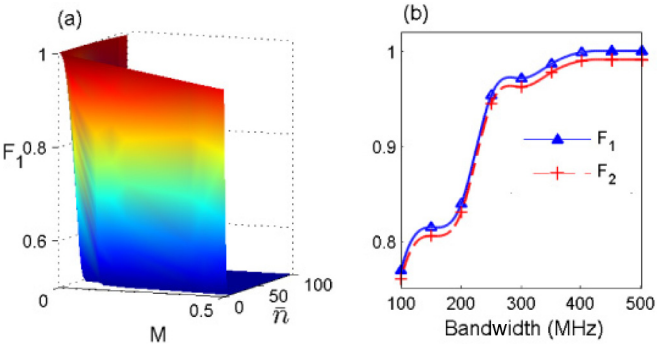

FIG. 5. (Color online) (a) Fidelity F_1 versus different values of the correction factor M and the average photon number $\bar{n}$. (b) Trajectories of the fidelities F_1 and F_2 versus different bandwidths of the signals. Both F_1 and F_2 can be very close to the ideal case, i.e., $F_1, F_2 \approx 1$ when the bandwidth of the signal is larger than 400 MHz, which means that we efficiently suppress the interference effects of our quantum CDMA network induced by the crosstalk between different data streams.

is the density operator of atoms 1 and 3 (atoms 2 and 4). In our simulations, we set $\phi = \pi/3$, where ϕ is the phase shift of the probe fields induced by the qubit-cavity coupling. The trajectories of the fidelity F_1 versus the correction factor M and the average photon number $\bar{n}$ are given in Fig. 5(a). We can see clearly that the fidelity F_1 can be very high if the factor M is small enough and $\bar{n}$ is not too small, which corresponds to our previous analysis. If we fix $\bar{n} = 10$ and increase the bandwidth of the signals, we can see the increase of the fidelities F_1 and F_2 as desired [see Fig. 5(b)]. Both F_1 and F_2 grow very quickly to approach 1 with the increase of the bandwidths of the signals to be larger than 400 MHz, which corresponds to a perfect entanglement distribution.

IV. NONIDEAL CASE: EFFECTS OF THE CHANNEL NOISE

In the previous sections we considered the ideal case in which the channel noises are omitted. To show the efficiency of our method in a more practical case, we consider the effects of the channel noises in this section [58,59]. The channel noises in quantum communication may come from different sources such as the vibration of the optical fiber used for transmitting quantum signals. Most of the channel noises, especially those induced by the fibers, are low-frequency noises with several to several hundreds of kHz, which is far smaller than the characteristic frequency of the information-bearing fields and also smaller than the frequency band of the chaotic phase shifts introduced by the chaotic circuits, which is typically of several hundreds MHz. For these reasons, we can omit the dynamical processes of the channel noises and simply believe that they act as a beam splitter to extract energy from the information-bearing field (see Fig. 6). As shown in Fig. 6, the input-output relationship of the beam splitter BS_3 used to represent the effects of the channel noises can be written as

$$a_7 = \sqrt{1-\eta}a_5 + \sqrt{\eta}a_{\rm ns}, \quad a_8 = \sqrt{1-\eta}a_5 - \sqrt{\eta}a_{\rm ns}, \quad (13)$$

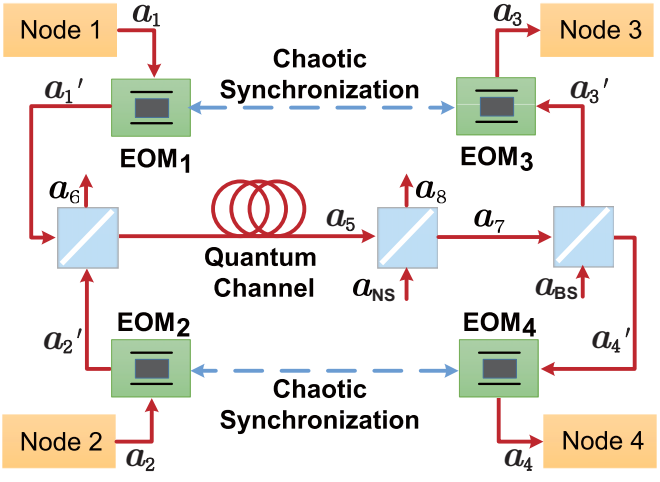

FIG. 6. (Color online) Schematic diagram of quantum CDMA network contains channel noise, where we use the beam splitter BS_3 to introduce channel noise.

where $a_{\rm ns}$ represents the noise mode and η denotes the decay rate induced by the noise. From Eqs. (1)–(6) and (13) we can obtain the input-output relationship of the noisy quantum CDMA network as

$$\begin{aligned} a_3 &= \frac{\sqrt{1-\eta}}{2}a_1 + \frac{\sqrt{(1-\eta)M_1M_2}}{2}a_2 + \sqrt{\frac{\eta M_1}{2}}a_{\rm ns} \\ &\quad + \sqrt{\frac{M_1}{2}}a_{\rm BS}, \\ a_4 &= \frac{\sqrt{1-\eta}}{2}a_2 + \frac{\sqrt{(1-\eta)M_1M_2}}{2}a_1 + \sqrt{\frac{\eta M_2}{2}}a_{\rm ns} \\ &\quad - \sqrt{\frac{M_2}{2}}a_{\rm BS}. \end{aligned}$$

If we further assume that the field $a_{\rm ns}$ is in a vacuum state, the output fields of the quantum CDMA network, i.e., a_3 and a_4, are in the coherent states

$$\begin{aligned} |\alpha_3\rangle &= \left|\frac{\sqrt{1-\eta}}{2}\alpha_1 + \frac{\sqrt{(1-\eta)M_1M_2}}{2}\alpha_2\right\rangle, \\ |\alpha_4\rangle &= \left|\frac{\sqrt{1-\eta}}{2}\alpha_2 + \frac{\sqrt{(1-\eta)M_1M_2}}{2}\alpha_1\right\rangle. \end{aligned} \quad (14)$$

Recall that the ith atom is in the superposition state $|\psi_i\rangle = (|g_i\rangle + |e_i\rangle)/\sqrt{2}$ and the probe field entering the cavity 1 (cavity 2) is a bright coherent light $|\alpha\rangle$ with average photon number $\bar{n} = |\alpha|^2 \gg 1$. By omitting the terms related to $\sqrt{M_1M_2}$ in Eq. (14), we can easily obtain the state of the total system composed of the four atoms and output fields of the quantum network as

$$\begin{aligned} |\Psi\rangle &= \left(\frac{1}{\sqrt{2}}|\Psi_{13}^+\rangle\left|\frac{\sqrt{1-\eta}}{2}\alpha\right\rangle + \frac{1}{2}|g_1g_3\rangle\left|\frac{\sqrt{1-\eta}}{2}\alpha e^{-i\phi}\right\rangle\right. \\ &\quad \left. + \frac{1}{2}|e_1e_3\rangle\left|\frac{\sqrt{1-\eta}}{2}\alpha e^{i\phi}\right\rangle\right) \\ &\quad \times \left(\frac{1}{\sqrt{2}}|\Psi_{24}^+\rangle\left|\frac{\sqrt{1-\eta}}{2}\alpha\right\rangle + \frac{1}{2}|g_2g_4\rangle\left|\frac{\sqrt{1-\eta}}{2}\alpha e^{-i\phi}\right\rangle\right. \\ &\quad \left. + \frac{1}{2}|e_2e_4\rangle\left|\frac{\sqrt{1-\eta}}{2}\alpha e^{i\phi}\right\rangle\right). \end{aligned}$$

If the decay rate η induced by the channel noise is not quite high and the probe fields are bright enough with average photon number $\bar{n} = |\alpha|^2 \gg 1/(1-\eta)$, we have

$$\begin{aligned} \left|\left\langle\frac{\sqrt{1-\eta}}{2}\alpha\left|\frac{\sqrt{1-\eta}}{2}\alpha e^{-i\phi}\right\rangle\right|^2 &= e^{-(1-\eta)\bar{n}\sin^2(\phi/2)} \approx 0, \\ \left|\left\langle\frac{\sqrt{1-\eta}}{2}\alpha\left|\frac{\sqrt{1-\eta}}{2}\alpha e^{i\phi}\right\rangle\right|^2 &= e^{-(1-\eta)\bar{n}\sin^2(\phi/2)} \approx 0, \\ \left|\left\langle\frac{\sqrt{1-\eta}}{2}\alpha e^{-i\phi}\left|\frac{\sqrt{1-\eta}}{2}\alpha e^{i\phi}\right\rangle\right|^2 &= e^{-(1-\eta)\bar{n}\sin^2\phi} \approx 0, \end{aligned}$$

which means that the three coherent states $|\sqrt{1-\eta}\alpha/2\rangle$, $|\sqrt{1-\eta}\alpha e^{-i\phi}/2\rangle$, and $|\sqrt{1-\eta}\alpha e^{i\phi}/2\rangle$ are pairwise orthogonal and thus completely distinguishable. Thus we can impose homodyne detections on the fields leaking out of cavities 3 and 4. If the corresponding measurement outputs for the two probe fields are both $\sqrt{1-\eta}\alpha/2$, the state of atoms 1 and 3

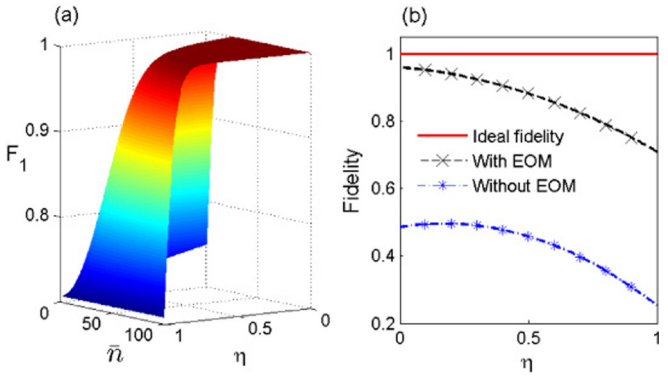

FIG. 7. (Color online) (a) Fidelity F_1 versus different decay rates η and the average photon number $\bar{n}$. (b) Trajectories of F_1 versus η with fixed $\bar{n} = 10$. The black dashed curve with plus signs shows the curve of the fidelity F_1 realized by our quantum CDMA network. The blue dash-dotted curve with asterisks represents the curve of F_1 when we the four EOMs are moved away. It is shown that our strategy can still be valid when we consider the channel noise if only the decay rate induced by the channel noises is not too high.

will collapse to the maximally entangled states $|\Psi_{13}^{+}\rangle$ and that of atoms 2 and 4 will collapse to the maximally entangled states $|\Psi_{24}^{+}\rangle$. From the above discussion we can conclude that our method is still valid if only the decay rate induced by the channel noise is not too high such that the decayed probe fields are still bright enough.

However, if the decay rate η induced by the channel noises is too high such that the average photon number $\bar{n} = |\alpha|^2$ is comparable to $1/(1-\eta)$, our entanglement distribution strategy will not be so perfect. In this case, we need to analyze the influence of noise on the fidelities F_1 and F_2. Without loss of generality, let us focus on the fidelity $F_1 = \langle\Psi_{13}^{+}|\rho_{13}|\Psi_{13}^{+}\rangle$ versus different decay rate η and average photon number $\bar{n}$. The discussion for the fidelity F_2 is quite similar and thus is omitted. We still choose $\phi = \pi/3$ and assume that the correction factors $M_1 = M_2 \approx 0$. With these system parameters, we show in Fig. 7 how the decay rate η affects the entanglement distribution. As can be seen from Fig. 7(a), fidelity F_1 can be very high when η is small and the average photon number is not large. Figure 7(b) shows the curves of the fidelity F_1 versus η for several different cases. The red solid curve represents the ideal case, i.e., $F_1 = 1$, which means that atoms 1 and 3 are in the maximally entangled state. The black dashed curve with plus signs denotes the trajectory of the fidelity F_1 with increasing η ranging from 0 to 1. The blue dash-dotted curve with asterisks shows the fidelity F_1 versus η without the four EOMs in our quantum CDMA network. By comparing these three curves, we can see that the fidelity F_1 will be greatly decreased if we move away the four EOMs in our quantum CDMA network. Meanwhile, with EOMs we can obtain a very high fidelity when the decay rate η is not too high.

V. CONCLUSION

We have presented a strategy to distribute quantum entanglement between two pairs of users via a single quantum channel. The interference of the quantum signals from different senders is greatly suppressed by introducing chaotic phase shifts to broaden the quantum signals in the frequency domain. It was shown that the two maximally entangled states can be generated between two pairs of nodes even when we consider the channel noises. It is hoped that our strategy could be applied to other systems such as solid-state quantum circuits and it would provide new perspectives for the field of quantum network control.

ACKNOWLEDGMENTS

C.L.Z. would like to thank Dr. R.B. Wu for helpful discussions. J.Z. and Y.X.L. were supported by the National Basic Research Program of China (973 Program) under Grant No. 2014CB921401, the NSFC under Grant No. 61328502 the Tsinghua University Initiative Scientific Research Program, and the Tsinghua National Laboratory for Information Science and Technology Cross-discipline Foundation. J.Z. was supported by the NSFC under Grants No. 61174084 and No. 61134008. Y.X.L. was supported by the NSFC under Grant No. 61025022. F.N. was partially supported by the RIKEN iTHES Project, MURI Center for Dynamic Magneto-Optics via the AFOSR Award No. FA9550-14-1-0040, the Impact Program of JST, and a Grant-in-Aid for Scientific Research (A).

APPENDIX A: CHAOTIC SYNCHRONIZATION OF COLPITTS OSCILLATOR CIRCUITS

In the system we consider, each pair of EOMs is driven by two standard chaotic Colpitts oscillator circuits [44], which are synchronized by the Pecora-Carroll synchronization strategy [45,46], as shown in Fig. 8. The Colpitts chaotic synchronization circuit comprises a transmitter and a receiver. The transmitter is a standard Colpitts oscillator circuit, which will enter the chaotic regime for particular system parameters. The receiver is a part of the standard Colpitts oscillator circuit. In our design, the system parameters of the Colpitts oscillator circuits, such as the resistance R, the inductance L, the capacitances C_1 and C_2, and the voltage V_{CC}, are chosen as $R = 27.99\Omega$, $L = 17.5$ nH, $C_1 = 13.1$ pF, $C_2 = 12.7$ pF, and $V_{CC} = 15$ V, under which the synchronized voltages V_{C2} and $\tilde{V}_{C2}$ are broadband chaotic signals with bandwidths of 500 MHz [45,46].

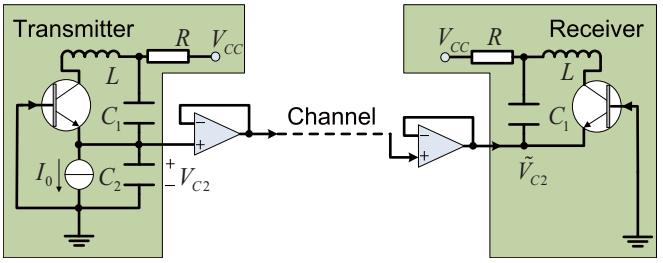

FIG. 8. (Color online) Schematic diagram of the synchronized chaotic Colpitts circuits, which is composed of a transmitter and a receiver. Here we adopt the Pecora-Carroll synchronization strategy to synchronize the two chaotic Colpitts circuits [47].

APPENDIX B: CALCULATIONS OF THE FIDELITIES OF ENTANGLED STATES

In this Appendix we present the calculations of the fidelity $F_1 = \langle\Psi_{13}^+|\rho_{13}|\Psi_{13}^+\rangle$. The calculations of the fidelity $F_2 = \langle\Psi_{24}^+|\rho_{24}|\Psi_{24}^+\rangle$ are similar to F_1, so we omit them. From Eq. (7) we see that if we consider the effect of the correction factor M, the state of the system composed of atoms 1 and 2 and those two probe fields that enter cavities 3 and 4 is

$$|\Phi\rangle = \tfrac{1}{2}|g_1g_2\rangle|\tfrac{1}{2}\alpha e^{-i\phi/2} + \tfrac{1}{2}M\alpha e^{-i\phi/2}\rangle|\tfrac{1}{2}\alpha e^{-i\phi/2} + \tfrac{1}{2}M\alpha e^{-i\phi/2}\rangle + \tfrac{1}{2}|g_1e_2\rangle|\tfrac{1}{2}\alpha e^{-i\phi/2} + \tfrac{1}{2}M\alpha e^{i\phi/2}\rangle|\tfrac{1}{2}\alpha e^{i\phi/2} + \tfrac{1}{2}M\alpha e^{i\phi/2}\rangle$$
$$+ \tfrac{1}{2}|e_1g_2\rangle|\tfrac{1}{2}\alpha e^{i\phi/2} + \tfrac{1}{2}M\alpha e^{-i\phi/2}\rangle|\tfrac{1}{2}\alpha e^{-i\phi/2} + \tfrac{1}{2}M\alpha e^{i\phi/2}\rangle + \tfrac{1}{2}|e_1e_2\rangle|\tfrac{1}{2}\alpha e^{i\phi/2} + \tfrac{1}{2}M\alpha e^{i\phi/2}\rangle|\tfrac{1}{2}\alpha e^{i\phi/2} + \tfrac{1}{2}M\alpha e^{i\phi/2}\rangle.$$

Then we can obtain the state of the total system composed of the four atoms and output fields of the quantum network as

$$|\Psi\rangle = e^{-i\left(H_3^{\mathrm{QC}}H_4^{\mathrm{QC}}\right)\tau}|\Phi\rangle\frac{1}{\sqrt{2}}(|g_3\rangle + |e_3\rangle)\frac{1}{\sqrt{2}}(|g_4\rangle + |e_4\rangle).$$

After the homodyne detections imposed on the probe fields leaking out of cavities 3 and 4, we can obtain the density operator ρ_{13} of atoms 1 and 3 by tracing out the degrees of freedom of atom 2, atom 4, and probe fields 3 and 4 by which the fidelity F_1 can be expressed as

$$\begin{aligned} F_1 &= \langle\Psi_{13}^+|\rho_{13}|\Psi_{13}^+\rangle \\ &= \tfrac{1}{2}(\langle e_1g_3| + \langle g_1e_3|)\rho_{13}(|e_1g_3\rangle + |g_1e_3\rangle) \\ &= \tfrac{1}{2} + \tfrac{1}{2}e^{-|\alpha|^2M^2(1-cos\phi)/2}, \end{aligned}$$

where $|\Psi_{13}^+\rangle$ is the maximally entangled state between atom 1 and atom 3 and the Hamiltonian H_i^{QC} is given in Eq. (9). From Eq. (5) we can calculate the correction factor M with respect to the bandwidths of the Colpitts circuits [see Fig. 4(a)], by which we can obtain the curve of F_1 versus the bandwidths of the Colpitts circuits.

[1] M. D. Lukin, Trapping and manipulating photon states in atomic ensembles, Rev. Mod. Phys. **75**, 457 (2003).

[2] L.-M. Duan and C. Monroe, Quantum networks with trapped ions, Rev. Mod. Phys. **82**, 1209 (2010).

[3] N. Sangouard, C. Simon, H. de Riedmatten, and N. Gisin, Quantum repeaters based on atomic ensembles and linear optics, Rev. Mod. Phys. **83**, 33 (2011).

[4] J. Q. You and F. Nori, Superconducting circuits and quantum information, Phys. Today **58**(11), 42 (2005).

[5] Y. Makhlin, G. Schön, and A. Shnirman, Quantum-state engineering with Josephson-junction devices, Rev. Mod. Phys. **73**, 357 (2001).

[6] Z. L. Xiang, S. Ashhab, J. Q. You, and F. Nori, Hybrid quantum circuits: Superconducting circuits interacting with other quantum systems, Rev. Mod. Phys. **85**, 623 (2013).

[7] H. J. Kimble, The quantum internet, Nature (London) **453**, 1023 (2008).

[8] M. A. Sillanpää, J. I. Park, and R. W. Simmonds, Coherent quantum state storage and transfer between two phase qubits via a resonant cavity, Nature (London) **449**, 438 (2007).

[9] X.-B. Wang, T. Hiroshima, A. Tomita, and M. Hayashi, Quantum information with Gaussian states, Phys. Rep. **448**, 1 (2007).

[10] J.-W. Pan, Z.-B. Chen, C.-Y. Lu, H. Weinfurter, A. Zeilinger, and M. Zukowski, Multi-photon entanglement and interferometry, Rev. Mod. Phys. **84**, 777 (2012).

[11] N. Gisin, G. Ribordy, W. Tittel, and H. Zbinden, Quantum cryptography, Rev. Mod. Phys. **74**, 145 (2002).

[12] M. Razavi, Multiple-access quantum key distribution networks, IEEE Trans. Commun. **60**, 3071 (2012).

[13] J. I. Cirac, P. Zoller, H. J. Kimble, and H. Mabuchi, Quantum State Transfer and Entanglement Distribution Among Distant Nodes in a Quantum Network, Phys. Rev. Lett. **78**, 3221 (1997).

[14] X. Maitre, E. Hagley, G. Nogues, C. Wunderlich, P. Goy, M. Brune, J. M. Raimond, and S. Haroche, Quantum Memory with a Single Photon in a Cavity, Phys. Rev. Lett. **79**, 769 (1997).

[15] D. F. Phillips, A. Fleischhauer, A. Mair, R. L. Walsworth, and M. D. Lukin, Storage of Light in Atomic Vapor, Phys. Rev. Lett. **86**, 783 (2001).

[16] L. M. Duan, M. D. Lukin, J. I. Cirac, and P. Zoller, Long-distance quantum communication with atomic ensembles and linear optics, Nature (London) **414**, 413 (2001).

[17] D. N. Matsukevich and A. Kuzmich, Quantum state transfer between matter and light, Science **306**, 663 (2004).

[18] A. Acín, J. I. Cirac, and M. Lewenstei, Entanglement percolation in quantum networks, Nat. Phys. **3**, 256 (2007).

[19] X.-Y. Lü, J. B. Liu, C. L. Ding, and J. H. Li, Dispersive atom-field interaction scheme for three-dimensional entanglement between two spatially separated atoms, Phys. Rev. A **78**, 032305 (2008).

[20] D. Felinto, C. W. Chou, J. Laurat, E. W. Schomburg, H. de Riedmatten, and H. J. Kimble, Conditional control of the quantum states of remote atomic memories for quantum networking, Nat. Phys. **2**, 844 (2006).

[21] C. H. van der Wal, M. D. Eisaman, A. Andre, R. L. Walsworth, D. F. Phillips, A. S. Zibrov, and M. D. Lukin, Atomic memory for correlated photon states, Science **301**, 196 (2003).

[22] C.-W. Chou, J. Laurat, H. Deng, K. S. Choi, H. de Riedmatten, D. Felinto, and H. J. Kimble, Functional quantum nodes for entanglement distribution over scalable quantum networks, Science **316**, 1316 (2007).

[23] T. Wilk, S. C. Webster, A. Kuhn, and G. Rempe, Single-atom single-photon quantum interface, Science **317**, 488 (2007).

[24] G. Smith and J. Yard, Quantum communication with zero-capacity channels, Science **321**, 1812 (2008).

[25] L. Czekaj and P. Horodecki, Purely Quantum Superadditivity of Classical Capacities of Quantum Multiple Access Channels, Phys. Rev. Lett. **102**, 110505 (2009).

[26] M. Demianowicz and P. Horodecki, Quantum channel capacities: Multiparty communication, Phys. Rev. A **74**, 042336 (2006).

[27] R. Rom and M. Sidi, *Multiple Access Protocols: Performance and Analysis* (Springer, New York, 1990).

[28] V. P. Ipatov, *Spread Spectrum and CDMA: Principles and Applications* (Wiley, London, 2005).

[29] L. E. Frenzel, *Principles of Electronics Communications Systems* (McGraw-Hill, New York, 2008).

[30] T. M. Cover and J. A. Thomas, *Elements of Information Theory* (Wiley, New York, 1991), p. 407.

[31] G. Brassard, F. Bussieres, N. Godbout, and S. Lacroix, Multiuser quantum key distribution using wavelength division multiplexing, Proc. SPIE **5260**, 149 (2003).

[32] P. Townsend, Simultaneous quantum cryptographic key distribution and conventional data transmission over installed fibre using wavelength-division multiplexing, Electron. Lett. **33**, 188 (1997).

[33] K. Yoshino, M. Fujiwara, A. Tanaka, S. Takahashi, Y. Nambu, A. Tomita, S. Miki, T. Yamashita, Z. Wang, M. Sasaki, and A. Tajima, High-speed wavelength-division multiplexing quantum key distribution system, Opt. Lett. **37**, 223 (2012).

[34] G. Brassard, F. Bussieres, N. Godbout, and S. Lacroix, in *Quantum Communication, Measurement and Computing*, edited by S. M. Barnett, O. Hirota, P. Öhberg, J. Jeffers, and E. Andersson, AIP Conf. Proc. No. 734 (AIP, New York, 2004), p. 323.

[35] I. Choi, R. J. Young, and P. D. Townsend, Quantum key distribution on a 10Gb/s WDM-PON, Opt. Express **18**, 9600 (2010).

[36] J. Roslund, R. Medeiros de Araujo, S. Jiang, C. Fabre, and N. Treps, Wavelength-multiplexed quantum networks with ultrafast frequency combs, Nat. Photon. **8**, 109 (2014).

[37] S. Yokoyama, R. Ukai, S. C. Armstrong, C. Sornphiphatphong, T. Kaji, S. Suzuki, J. Yoshikawa, H. Yonezawa, N. C. Menicucci, and A. Furusawa, Ultra-large-scale continuous-variable cluster states multiplexed in the time domain, Nat. Photon. **7**, 982 (2013).

[38] F. Li, L. Z. Zhou, L. Liu, and H. B. Li, in *Proceedings of the 18th International Conference on Telecommunications* (IEEE, Piscataway, 2011), p. 276.

[39] M. Anandan, S. Choudhary, and K. P. Kumar, in *Proceedings of the International Conference on Fibre Optics and Photonics* (OSA, Washington, DC, 2012), p. 3.

[40] J. Zhang, Y.-X, Liu, S. K. Özdemir, R.-B. Wu, F. F. Gao, X.-B. Wang, L. Yang, and F. Nori, Quantum internet using code division multiple access, Sci. Rep. **3**, 2211 (2013).

[41] J. C. Garcia-Escartin and P. Chamorro-Posada, Quantum spread spectrum multiple access, IEEE J. Sel. Top. Quantum Electron. **21**, 6400107 (2015).

[42] T. S. Humble, Quantum spread spectrum communication, Proc. SPIE **8057**, 80570J (2011).

[43] J. C. Garcia-Escartin and P. Chamorro-Posada, Quantum multiplexing with optical coherent states, Quantum Inf. Comput. **9**, 573 (2009).

[44] M. P. Kennedy, Chaos in the Colpitts oscillator, IEEE Trans. Circuit Syst. **41**, 771 (1994).

[45] Z. G. Shi and L. X. Ran, Microwave chaotic Colpitts oscillator: Design, implementation and applications, J. Electromagn. Waves Appl. **20**, 1335 (2006).

[46] U. Parlitz, L. O. Chua, Lj. Kocarev, K. S. Halle, and A. Shang, Transmission of digital siganls by chaotic synchronization, Int. J. Bifurcat. Chaos **02**, 973 (1992).

[47] L. M. Pecora and T. L. Carroll, Synchronization in Chaotic Systems, Phys. Rev. Lett. **64**, 821 (1990).

[48] K. M. Cuomo and A. V. Oppenheim, Circuit Implementation of Synchronized Chaos with Applications to Communications, Phys. Rev. Lett. **71**, 65 (1993).

[49] J. Zhang, Y.-X. Liu, W.-M. Zhang, L.-A. Wu, R.-B. Wu, and T.-J. Tarn, Deterministic chaos can act as a decoherence suppressor, Phys. Rev. B **84**, 214304 (2011).

[50] L. Zhou, S. Yang, Y. X. Liu, C. P. Sun, and F. Nori, Quantum Zeno switch for single-photon coherent transport, Phys. Rev. A **80**, 062109 (2009).

[51] S. Ashhab, J. R. Johansson, A. M. Zagoskin, and F. Nori, Two-level systems driven by large-amplitude fields, Phys. Rev. A **75**, 063414 (2007).

[52] J. Bergli, Y. M. Galperin, and B. L. Altshuler, Decoherence in qubits due to low-frequency noise, New J. Phys. **11**, 025002 (2009).

[53] P. van Loock, T. D. Ladd, K. Sanaka, F. Yamaguchi, K. Nemoto, W. J. Munro, and Y. Yamamoto, Hybrid Quantum Repeater Using Bright Coherent Light, Phys. Rev. Lett. **96**, 240501 (2006).

[54] T. D. Ladd, P. van Loock, K. Nemoto, W. J. Munro, and Y. Yamamoto, Hybrid quantum repeater based on dispersive CQED interactions between matter qubits and bright coherent light, New J. Phys. **8**, 184 (2006).

[55] A. Blais, R. S. Huang, A. Wallraff, S. M. Girvin, and R. J. Schoelkopf, Cavity quantum electrodynamics for superconducting electrical circuits: An architecture for quantum computation, Phys. Rev. A **69**, 062320 (2004).

[56] P. Kolchin, C. Belthangady, S. W. Du, G. Y. Yin, and S. E. Harris, Electro-Optic Modulation of Single Photons, Phys. Rev. Lett. **101**, 103601 (2008).

[57] M. Tsang, Cavity quantum electro-optics, Phys. Rev. A **81**, 063837 (2010).

[58] J. Jing and T. Yu, Non-Markovian Relaxation of a Three-Level System: Quantum Trajectory Approach, Phys. Rev. Lett. **105**, 240403 (2010).

[59] J. Jing, L. A. Wu, M. Byrd, J. Q. You, T. Yu, and Z. M. Wang, Nonperturbative Leakage Elimination Operators and Control of a Three-Level System, Phys. Rev. Lett. **114**, 190502 (2015).